ARTICLE
Traditional Medicine Research 2025;10(4):20. https://doi.org/10.53388/TMR20240925001

KEAP1 inhibitor-scutellarin-based liposomes serve as an antioxidant switch for oxidative stress induced by ischemic stroke injury

Kai-Rui Liu[1#], Jun-Li Ba[1#], Yun Wang[2#], Sheng-Tao Hu[1], Lu Gao[3], Xiao-Ning Gao[1*], Chang-Hua Kou[2*], Jun Kang[1*]

[1]School of Life Sciences, Faculty of Medicine, Tianjin University, Tianjin 300072, China. [2]Hepatobiliary Pancreatic Center, Xuzhou Central Hospital, Xuzhou 221009, China. [3]School of Basic Medical Science, Beijing Health Vocational College, Beijing 102402, China.

[#]These authors contributed equally to this work and are co-first authors for this paper.
[*]**Correspondence to:** Xiao-Ning Gao, Jun Kang. School of Life Sciences, Faculty of Medicine, Tianjin University, No. 92, Wei-jin Avenue, Tianjin 300072, China. E-mail: xiaoninggao@tju.edu.cn; jun.kang@tju.edu.cn. Chang-Hua Kou, Hepatobiliary Pancreatic Center, Xuzhou Central Hospital, No. 199, Jie-fang South Avenue, Xuzhou 221009, China. E-mail: kouchanghua@126.com.

Author contributions
Liu KR and Ba JL contributed to the experimental design and data collection. Wang Y was involved in data analysis and interpretation. Hu ST and Gao L provided technical support. Gao XN, Kou CH and Kang J supervised the overall project and were responsible for manuscript writing and final approval of the version to be published.

Competing interests
The authors declare no conflicts of interest.

Acknowledgments
This project was financially supported by the Medical and Health Project (2023, No. KC23178).

Peer review information
Traditional Medicine Research thanks Liu Tian-Long and other three anonymous reviewers for their contribution to the peer review of this paper.

Abbreviations
KEAP1, Kelch-like ECH-associated protein 1; NRF2, nuclear factor E2-related factor 2; HO-1, heme oxygenase 1; NQO1, NAD(P)H quinone dehydrogenase 1; ROS, reactive oxygen species; DPPC, 1,2-dipalmitoyl-sn-glycero-3-phosphocholine; DSPE-PEG2000, 1,2-distearoyl-sn-glycero-3-phosphoethanolamine-poly(ethylene glycol)-2000; DMEM, Dulbecco's modified Eagle's medium; HDX-MS, hydrogen-deuterium exchange mass spectrometry; GO, Gene Ontology; RhB, Rhodamine B; ARE, antioxidant response element; TNF, tumor necrosis factor; GSTP1, glutathione S-transferase pi 1; SRC, proto-oncogene tyrosine-protein kinase src; MAPK14, mitogen-activated protein kinase 14; CASP8, caspase-8; GAPDH, glyceraldehyde-3-phosphate dehydrogenase.

Citation
Liu KR, Ba JL, Wang Y, et al. KEAP1 inhibitor-scutellarin-based liposomes serve as an antioxidant switch for oxidative stress induced by ischemic stroke injury. *Tradit Med Res.* 2025;10(4):20. doi: 10.53388/TMR20240925001.

Executive editor: Xin-Yue Zhang.
Received: 26 September 2024; **Revised:** 27 October 2024; **Accepted:** 24 December 2024; **Available online:** 27 December 2024.

Abstract

Background: Ischemic stroke is a disease characterized by the damage of brain tissue due to insufficient blood supply. The neuronal necrosis caused by oxidative stress during the acute phase of ischemic stroke leads to serious consequences, including blood-brain barrier disruption and vascular aging. The Kelch-like ECH-associated protein 1 (KEAP1), is a key switch of antioxidative system in human body. Until now, there is still a lack of effective treatment to ischemic stroke. **Methods:** We developed scutellarin-based liposomes for treating ischemic stroke injury caused neuronal damage. **Results:** The results showed that scutellarin could directly bind to KEAP1 protein, and the Kd was 26.1 μM. The scutellarin-based liposomes significantly reduced cellular reactive oxygen species (ROS) levels. It could also upregulate the protein expression level of nuclear factor E2-related factor 2 (NRF2), which is the substrate protein of KEAP1. Next, both the mRNA and protein expression level of the NRF2 downstream anti-oxidative element, heme oxygenase 1 (HO-1) and NAD(P)H quinone dehydrogenase 1 (NQO1) were promoted. Furthermore, the coimmunoprecipitation (Co-IP) and hydrogen-deuterium exchange mass spectrometry (HDX-MS) revealed that scutellarin directly bound to KEAP1's Kelch domain, interrupting the interaction between KEAP1 and NRF2. **Conclusion:** Our work indicates that the scutellarin-based liposomes might be a promising therapeutic approach for ischemic stroke induced neuronal necrosis.

Keywords: oxidative stress; scutellarin; liposomes; KEAP1; NRF2

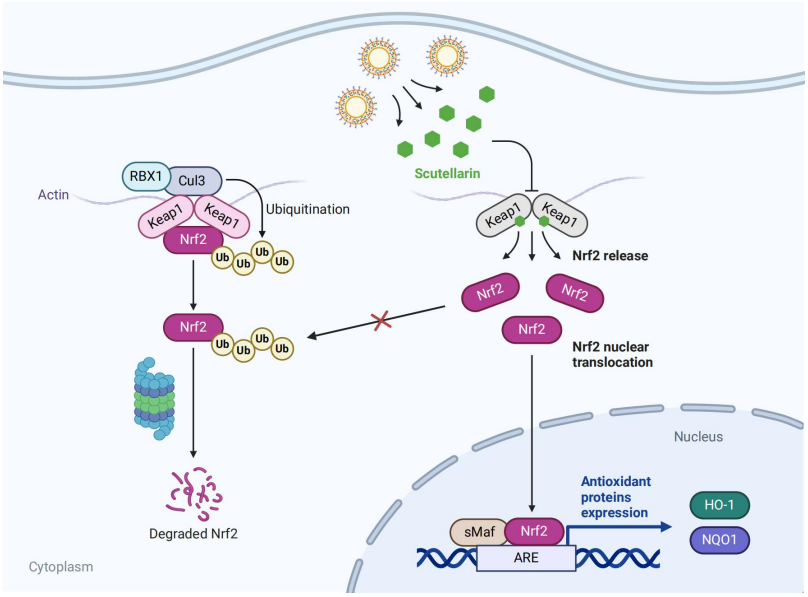

Highlights

Scutellarin-based liposomes with KEAP1 inhibitor were developed for the treatment of neuronal damage caused by ischemic stroke.

Experiments showed that scutellarin liposomes significantly reduced intracellular reactive oxygen species levels and upregulated the expression of antioxidant-related proteins, effectively alleviating oxidative stress.

The study confirmed that scutellarin directly binds to the Kelch domain of KEAP1, interfering with the interaction between KEAP1 and NRF2, revealing its mechanism of action as an antioxidant switch.

Medical history of objective

Scutellarin, a flavonoid with antioxidant and other properties, comes from herbs like *Scutellaria baicalensis*. In traditional medicine, these herbs are for heat-clearing (a therapeutic method that aims to expel excessive internal heat in the body). No direct scutellarin record in old books, but *Scutellaria baicalensis* is in *Shennong's Classic of Materia Medica* (25–220 C.E.). Now, scutellarin helps with cell damage, interacts with disease pathways.

Introduction

Stroke stands as the second leading cause of death globally and the primary source of permanent disability [1, 2]. Ischemic stroke, in particular, is linked with high incidence, disability rates, and mortality [3]. During ischemic stroke, the deprivation of oxygen and glucose in brain tissue initiates the production of inflammatory factors and reactive oxygen species (ROS), especially superoxide radicals [4–6]. These elements lead to neuronal degeneration and severe tissue damage, resulting in substantial cytotoxicity [7, 8]. Current clinical treatments for ischemic stroke center on restoring blood flow through intravenous thrombolysis and endovascular therapy, complemented by antioxidants and anti-inflammatory agents for neuroprotection [9–11]. However, the only Food and Drug Administration (FDA)-approved thrombolytic agent, rt-PA, has a restricted therapeutic window [12]. Additionally, small molecule antioxidants and other drugs have significant limitations, highlighting the urgent need for safer, more effective long-acting therapies and advanced drug delivery methods.

Scutellarin is a flavonoid compound found in traditional Chinese medicinal herbs such as *Scutellaria baicalensis*, *Ligusticum chuanxiong*, and *Andrographis paniculata* [13, 14]. Over the past three decades, research has shown that scutellarin exhibits antioxidant, anti-inflammatory, anticancer, and neuroprotective properties [15–17]. These effects are particularly notable in addressing oxidative stress damage in vascular endothelial cells, apoptosis induced by oxidants and ischemia-reperfusion injury in cardiomyocytes [18–20]. Scutellarin also interacts with various signaling pathways relevant to cerebrovascular and cardiovascular diseases [21–23]. Despite these promising attributes, the exact antioxidant mechanisms of scutellarin remain incompletely understood, posing challenges for its further development. Additionally, scutellarin's low water solubility, poor oral bioavailability, and short half-life further complicate its development and practical application [24].

Liposomes are a highly recommended drug delivery system, widely endorsed by the FDA [25]. Their small particle size, amphiphilic nature, and excellent biocompatibility contribute to high drug-loading efficiency, enhanced drug stability and bioavailability, and reduced systemic toxicity [26–28]. These characteristics help minimize adverse reactions and boost therapeutic efficacy [29, 30]. The phospholipid structure of liposomes ensures effective interaction with mammalian cell membranes, facilitating cellular uptake [31, 32]. Encapsulating scutellarin in liposomes (approximately 100 nm in size) can overcome its poor solubility, low bioavailability, and short half-life, thereby expanding its potential for clinical applications.

Here, we developed scutellarin-based liposomes, which enhanced its bioavailability and biocompatibility, serving as an antioxidant switch to alleviate ischemic stroke injury. Experiments demonstrated that these scutellarin-based liposomes effectively reduced cellular ROS levels, alleviated oxidative stress, and mitigated ischemic stroke injury. Additionally, mRNA and protein expression analyses revealed that scutellarin-based liposomes can upregulate nuclear factor E2-related factor 2 (NRF2) protein expression, thereby activating downstream antioxidant elements such as heme oxygenase 1 (HO-1) and NAD(P)H quinone dehydrogenase 1 (NQO1). Co-immunoprecipitation and hydrogen-deuterium exchange mass spectrometry showed that scutellarin directly binds to the Kelch domain of the Kelch-like ECH-associated protein 1 (KEAP1), allosterically regulating KEAP1 and influencing its interaction with the NRF2 protein, thus enabling its role as an antioxidant switch.

Material and methods

Reagents and chemicals

Scutellarin (Sut) (CAS: 27740-01-8, Cat No. Y-012-5g) was purchased from Chengdu Herbpurify (Chengdu, China). Tert-Butyl hydroperoxide (CAS: 75-91-2, Cat No. B802372-50ml) was purchased from Macklin (Shanghai, China). 1,2-dipalmitoyl-sn-glycero-3-phosphocholine (DPPC) (CAS: 63-89-8, Cat No. HY-109506), 1,2-distearoyl-sn-glycero-3-phosphoethanolamine-poly(ethylene glycol)-2000 (DSPE-PEG2000) (CAS: 892144-24-0, Cat No. HY-142979) and cholesterol (CAS: 57-88-5, Cat No. HY-N0322) were purchased from MedChemExpress (Shanghai, China). Primary antibodies of anti-KEAP1 (Cat No. 30041-1-AP), anti-NRF2 (Cat No. 16396-1-AP), anti-HO-1 (Cat No. 10701-1-AP), anti-NQO1 (Cat No. 11451-1-AP), anti-GAPDH (Cat No. 60004-1-Ig), anti-Tubulin (Cat No. 66240-1-Ig), anti-Flag (Cat No. 80010-1-RR) were purchased from Proteintech (Wuhan, China). anti-Flag affinity matrix (Cat No. A2220) was purchased from Sigma (Shanghai, China). The enhanced chemiluminescence reagent (Cat No. SQ201) was purchased from EpiZyme (Shanghai, China). Reactive oxygen species assay kit (Cat No. CA1410), Hoechst 33342 Stain solution (Cat No. C0031-1ml), and CCK-8 cell proliferation and cytotoxicity assay kit (Cat No. CA1210) were purchased from Solarbio Life Science (Beijing, China). Recombinant human KEAP1 protein was purchased from Sino Biological (Beijing, China) (Cat No. 11981-HNCB).

Preparation of sut-liposome

DPPC, DSPE-PEG2000, and cholesterol were each dissolved in chloroform and methanol (2:1 v/v) to prepare stock solutions with concentrations of 100 mg/mL, 50 mg/mL, and 10 mg/mL, respectively. To dissolve 1 mg of scutellarin, 60 μL DPPC, 40 μL DSPE-PEG2000, and 25 μL cholesterol, 3 mL of chloroform and methanol mixture (3:1 v/v) was added into a 25 mL round-bottom flask. The components were thoroughly and uniformly mixed before securing the flask on a vacuum rotary evaporator. The rotation speed was set to 15 rpm, with the water bath temperature maintained at 30 °C, and the vacuum pump activated to facilitate the removal of the organic solvent. After 20 min of rotary evaporation, a uniform thin film formed on the sidewall of the flask. To hydrate the lipid film and form liposomes, 3 mL of PBS buffer solution was slowly added to the flask, followed by sonication for 7 min. The resulting hydrated liposome solution was extruded using a liposome extruder (Avanti, Birmingham, AL, USA), sequentially passing through polycarbonate filters of 400 nm and 200 nm to obtain scutellarin-loaded liposomes with uniform particle sizes. The extrusion process was maintained at a constant speed. Post-preparation, the liposomes were stored at 4 °C for subsequent use.

Characterization of sut-liposome

Particle size and potential measurement. The particle size distributions of the liposomes were determined by dynamic light scattering, and the superficial charge was expressed as zeta potential

(ζ). These measurements were performed on undiluted samples using a Malvern Zetasizer (Zeta PALS, Brookhaven, Rockville, MD, USA). The morphology and size of the liposomes were examined by transmission electron microscopy (FEI TECNAI G2 F30, FEI, Hillsboro, OR, USA).

Encapsulation efficiency determination. The encapsulation efficiency (EE) of scutellarin and drug loading capacity (DLC) were calculated using the formulas EE (%) = $[C_{encapsulation}/C_{total}] \times 100\%$ and DLC (%) = $[W_e/W_m] \times 100\%$, where C_{total} is the initial scutellarin concentration, $C_{encapsulation}$ is the concentration of encapsulated scutellarin, and is the quantity of drug in the pharmaceutical preparation. W_e represents the quantity of drug in the pharmaceutical preparation, while W_m stands for the total mass of the preparation. To prepare a 2 mM stock solution, 0.9 mg of scutellarin was weighed and dissolved in 1 mL of anhydrous methanol. After gradient dilution of this stock solution, the absorbance at 335 nm was measured using a UV-Vis spectrophotometer (Shimadzu, Shanghai, China) to plot a standard curve for scutellarin. The Sut-liposome obtained from the first synthesis was centrifuged at 6 ˚C and 8,000 rpm for 10 min, and the supernatant was discarded. Methanol (2 mL) was added to disrupt the liposomes, ensuring complete dissolution of the encapsulated scutellarin. The solution was then loaded onto an Agilent Captiva EMR-Lipid filtration column (Agilent, Shanghai, China), allowed to stand for 5 min, and the liquid was expressed using a syringe to remove lipid molecules, yielding a scutellarin solution. The absorbance at 335 nm was measured using a UV-Vis spectrophotometer, and the encapsulation efficiency and drug loading were calculated using the standard curve.

Cell culture

HT22 cells, HEK 293T cells, and SH-SY5Y cells (Pricella, Wuhan, China) were cultured in Dulbecco's modified Eagle's medium (DMEM) supplemented with 15% fetal bovine serum and 1% double-antibody. Cells were maintained at 37 ˚C in a 5% CO_2 incubator. When the cell growth density reached 90%, they were digested and passaged with 0.25% trypsin and then inoculated into new culture bottles for subsequent experiments.

Endocytosis assay

According to the aforementioned liposomes preparation method, liposomes loaded with Rhodamine B (RhB) were prepared by hydrating the lipid film with PBS buffer containing Rhodamine B at a concentration of 0.3 mg/mL. The solution was stirred and dialyzed in PBS buffer for 24 h to remove unencapsulated Rhodamine B. HT22 cells were seeded in a 12-well plate, and Rhodamine B-loaded liposomes (10 μL per well) were added to the cells. Hoechst 33342 dye diluted in DMEM (1:100) was then added. The plate was incubated at 37 ˚C in the dark for 15 min, after which the dye-containing medium was aspirated, and each well was washed three times with 500 μL of PBS. Finally, 500 μL of DMEM was added, and cellular uptake was observed at 1, 3, and 6 h post-addition of the Rhodamine B-loaded liposomes using a laser confocal microscope.

CCK-8 cell viability and cytotoxicity assay

HT22 cells were cultured in 96-well plates for CCK-8 experiments. After culturing for more than 24 h, when cell confluence reached 80%, sut-liposome were added at varying concentrations for treatment, with triplicate sets for each group. Three repeats were set for each group. CCK-8 solution was added, and the cells were cultured for 0.5 h until a visible yellow color change occurred. The absorbance at 450 nm was detected using a microplate reader.

ROS generation determination

Intracellular ROS levels were tested in HT22 cells cultured on a 12-well plate and incubated at 37 ˚C under 5% CO_2. After pretreatment with sut-liposome for 3 h and subsequent incubation with tert-butyl hydroperoxide for 6 h, DCFM-DA and Hoechst 33342 were added, followed by a 12-min incubation in the dark at 37 ˚C. The cells were then collected, washed three times with PBS, and ROS activity was detected using an inverted fluorescence microscope.

Relative quantification of mRNA by real-time PCR

Total RNA extraction and reverse transcription. Total RNA from HT22 cells was extracted using Trizol lysis reagent (Solarbio Life Science, Beijing, China). RNA was reverse transcribed into cDNA using TransScript® Uni All-in-One First-Strand cDNA Synthesis SuperMix for qPCR (AU341-02, Transgen, Beijing, China), strictly following the kit's instructions. The first strand of cDNA was synthesized at 42–65 ˚C. The kit contains DNase to remove genomic DNA from RNA templates. The prepared cDNA was stored on ice for subsequent steps.

qPCR Primers:

GAPDH-F: 5'-AGGTCGGTGTGAACGGATTTG-3'

GAPDH-R: 5'-GGGGTCGTTGATGGCAACA-3'

Hmox1-F: 5'-GGGGTCGTTGATGGCAACA-3'

Hmox1-R: 5'-CATCACCAGCTTAAAGCCTTCT-3'

Nqo1-F: 5'-AGGATGGGAGGTACTCGAATC-3'

Nqo1-R: 5'-TGCTAGAGATGACTCGGAAGG-3'

qPCR reaction steps. Gene expression levels were detected using Hieff® qPCR SYBR Green Master Mix (Yeasen, Shanghai, China) on a CFX96 real-time PCR instrument (Bio-Rad, Shanghai, China). Glyceraldehyde-3-phosphate dehydrogenase (GAPDH) expression was used as an internal reference, with three replicates per sample. The reaction system included 8 μL of 2× SYBR Green mix, 0.4 μL of template cDNA, 2 μL of primers (1.5 μM each), and 5.6 μL of ddH_2O.

Western blotting

After the specified treatment period, cells and supernatants were collected directly into centrifuge tubes. Following centrifugation at 6,500 rpm for 5 min at 4 ˚C, the cells were washed three times with PBS and lysed in RIPA buffer. Protein samples were then separated using 12% SDS-PAGE and transferred to nitrocellulose membranes. The membranes were blocked with 5% skimmed milk for 30 min at room temperature and incubated overnight at 4 ˚C with primary antibodies. All primary antibodies, including anti-KEAP1, anti-NRF2, anti-HO-1, anti-NQO1, anti-FLAG, anti-GAPDH, and anti-Tubulin, were diluted at a ratio of 1:1,000. The membranes were washed three times with TBST (120 rpm, 6 min per wash) and then exposed to horseradish peroxidase-conjugated secondary antibodies (60 rpm, 60 min). The primary antibodies anti-KEAP1, anti-NRF2, anti-HO-1, anti-NQO1, and anti-FLAG were rabbit-derived, while anti-GAPDH and anti-Tubulin were mouse-derived. Secondary antibodies, either goat anti-rabbit or goat anti-mouse, were selected according to the source of the primary antibodies, with all secondary antibodies diluted at a ratio of 1:5,000. Signals were detected using enhanced chemiluminescence reagent, and fold changes in protein levels were analyzed using ImageJ software.

Ligand fishing

Epoxy-activated SepharoseTM 6B microspheres were pre-washed in PBS buffer, mixed with scutellarin solution or solvent, and incubated at 30 ˚C for 16 h. SH-SY5Y cells were lysed with cell lysis buffer, and the supernatant was incubated with the drug-coupled medium overnight at 4 ˚C. The medium was then washed three times with PBS, and the samples were boiled in SDS loading buffer. The target proteins were separated by protein gel electrophoresis and visualized by silver staining. Specific proteins were identified by mass spectrometry.

Bio-layer interferometry assay (BLI)

The Octet RED96e system (Molecular Device, ForteBIO, Shanghai, China) was used to characterize the binding kinetics and affinity between proteins and small molecules. Both wild-type and mutant Kelch proteins were purified, biotinylated, and diluted to a concentration of 50 μg/mL. These proteins were then immobilized on SSA sensors. After blocking and washing, the sensors were placed in wells containing different concentrations of scutellarin in a kinetic buffer. Program settings default to programs that bind proteins and small molecules in the system. Binding signals were recorded and analyzed using OctetHT V10.0 software. The goodness of fit (R^2) was

calculated, with values close to 1 indicating an excellent fit.

Coimmunoprecipitation (Co-IP)

HEK 293T cells were inoculated into four 6 cm dishes and pre-cultured in an incubator at 37 ˚C with 5% CO_2 for 24 h. The cells were then transfected with pcDNA3.1 or KEAP1-FLAG plasmid using polyethyleneimine reagent. The drug treatment group was incubated with 30 μM scutellarin for 3 h. After incubation, adherent cells were collected into centrifuge tubes and lysed in 700 μL lysis buffer for 60 min on ice. The lysate was then centrifuged at 12,000 rpm for 30 min, and the supernatant was transferred to a new centrifuge tube. anti-FLAG affinity matrix (40 μL) was added to the supernatant and incubated overnight at 4 ˚C. After incubation, the lysates were washed three times with PBS, and the supernatant was discarded. The proteins were eluted with glycine buffer (pH = 2), boiled in SDS loading buffer, and analyzed by western blotting.

Hydrogen-deuterium exchange mass spectrometry (HDX-MS)

Purified Kelch protein (a structural domain of the KEAP1 protein) was pre-incubated with scutellarin or DMSO at 4 ˚C overnight. After dilution with D2O buffer, the protein was equilibrated and quenched with an ice-cold buffer. The quenched sample was rapidly digested with immobilized pepsin and desalted using a C18 column. Peptide separation was achieved on a Thermo-Dionex Ultimate 3000 HPLC system, and mass spectrometry was performed using a Thermo Scientific Q Exactive system. The raw data were processed using Proteome Discoverer software, and the degree of deuterium incorporation in peptides was analyzed using HDExaminer software.

Network pharmacology analysis

Target Collection. The chemical structure and CAS number of scutellarin (CAS number 27740-01-8) were used to retrieve target data from PubChem (https://pubchem.ncbi.nlm.nih.gov/), Swiss Target Prediction (http://www.swisstargetprediction.ch/) and PharmMapper were employed to predict potential targets of scutellarin, while ischemic stroke-related targets were identified using databases such as OMIM (http://omim.org/), GeneCards (http://www.genecards.org/), DrugBank, and TTD.

PPI Network Construction. A Venn diagram was created to compare the intersection of scutellarin and ischemic stroke targets. The intersecting targets were imported into the STRING database (https://string-db.org/) to construct a protein-protein interaction (PPI) network. The network was analyzed to identify key proteins.

GO and KEGG analysis. Gene Ontology (GO) was performed using the DAVID database (https://string-db.org/) to determine the potential biological processes, cellular components, molecular functions, and Kyoto Encyclopedia of Genes and Genomes (KEGG) pathway enrichment analysis identifies key pathways related to the treatment of ischemic stroke that are influenced by scutellarin.

Statistical analysis

All results were analyzed with GraphPad Prism 10 and are presented as mean values ± SD. Statistical significance was determined using the Student's T test or one-way ANOVA test. The statistical significance was indicated at a P value < 0.05. (ns, no significance; $^{*}P < 0.05$; $^{**}P < 0.01$; $^{***}P < 0.001$; $^{****}P < 0.0001$).

Results

Network pharmacology analysis and molecular

Network pharmacology analysis was conducted to identify potential targets of scutellarin in the treatment of ischemic stroke. A total of 144 target proteins related to scutellarin were identified, and 1,105 ischemic stroke-related targets were obtained. Intersection analysis yielded 49 potential targets for further exploration (Figure 1A). PPI network analysis of these targets, conducted using the STRING tool, revealed a network of 49 nodes and 267 edges. The topological analysis identified the top 10 core targets, including GSTP1, proto-oncogene tyrosine-protein kinase src (SRC), tumor necrosis factor (TNF), mitogen-activated protein kinase 14 (MAPK14), caspase-8 (CASP8), etc. (Figure 1B). GO functional analysis (Figure 1C) and KEGG pathway enrichment implicated (Figure 1D) key biological processes such as inflammatory response regulation and ROS metabolism, with significant involvement in the MAPK, NF-κB, and TNF signaling pathways. The biological functions obtained by GO analysis and the main proteins of relative pathways were selected in the network (Figure 1E). The main proteins in the pathway obtained by GO analysis were selected for molecular docking with scutellarin. Although not in the enrichment results, KEAP1, a key factor in the antioxidant pathway, also underwent molecular docking. Use CB-dock2 software to predict the molecular docking location of scutellarin and six proteins, including KEAP1, GSTP1, SRC, TNF, MAPK14, and CASP8. And the lowest free energy conformation was selected for docking (Figure 2A–2F). The Vina score provided by the website indicates the binding energy of protein and scutellarin docking. Outcomes are selected based on the lowest binding energy. Specifically, KEAP1 and scutellarin show a vina score of −10.3 kcal/mol; GSTP1 and scutellarin have a vina score of −7.7 kcal/mol; SRC and scutellarin present a vina score of −9.7 kcal/mol; TNF and scutellarin exhibit a vina score of −6.7 kcal/mol; MAPK14 and scutellarin show a vina score of −7.6 kcal/mol; and CASP8 and scutellarin have a vina score of −7.1 kcal/mol.

Preparation and characterization of scutellarin liposomes

Scutellarin liposomes were synthesized using the thin-film hydration method, followed by extrusion through 400 nm and 200 nm polycarbonate membranes. The resulting scutellarin liposomes were characterized for morphology, particle size, and stability. Transmission electron microscopy (TEM) confirmed the spherical morphology of the liposomes (Figure 3A). Dynamic light scattering analysis revealed an average particle size of 126.5 nm with a polydispersity index of 0.179, indicating a uniform and narrow size distribution (Figure 3B). The Zeta potential, measured at 25 ˚C in an aqueous solution at pH 7, averaged −39.7 mV (Figure 3C), suggesting good colloidal stability. The UV-visible absorption spectrum of scutellarin liposomes showed a peak at 335 nm, corresponding to the characteristic absorption peak of free scutellarin, confirming successful encapsulation within the liposomal structure (Figure 3D). Scutellarin's UV absorption peaks at 285 nm and 335 nm were used to establish a standard curve for quantifying encapsulation efficiency. The absorbance at 335 nm was selected due to its stronger correlation with scutellarin concentration. Post-filtration, the lysed liposomal solution was diluted 10-fold, yielding an absorbance value of 2.42 at 335 nm. Applying this value to the standard curve, the encapsulation efficiency of scutellarin in the liposomes was calculated to be 88.77%, with a drug loading efficiency of 8.98%. Stability studies in various media, including ddH_2O, phosphate-buffered saline, and culture medium supplemented with 10% fetal bovine serum, demonstrated that the average particle size change over a 14-day period remained below 10%, indicating excellent stability under both physiological and non-physiological conditions (Figure 3E).

To assess cellular uptake, RhB was encapsulated within the liposomes, and fluorescence microscopy was used to monitor internalization in HT22 cells. Cell nuclei were counterstained with Hoechst 33342 (blue fluorescence), while RhB provided a red fluorescence signal indicative of liposome presence. One hour post-incubation, minimal red fluorescence was detected within the cells. However, after 3 h, there was a significant increase in intracellular red fluorescence, which further intensified at 6 h, confirming efficient endocytosis of scutellarin liposomes by HT22 cells (Figure 3G). The cytotoxicity of scutellarin liposomes on HT22 cells was evaluated using the CCK-8 assay. HT22 cells were treated with scutellarin liposomes at concentrations ranging from 10 to 150 μL/mL. The results demonstrated that cell viability remained above 95% across all tested concentrations, with no significant decrease observed even at the highest concentration of 150 μL/mL. This indicates that scutellarin liposomes are non-cytotoxic to normal cells within the experimental concentration range (Figure 3F).

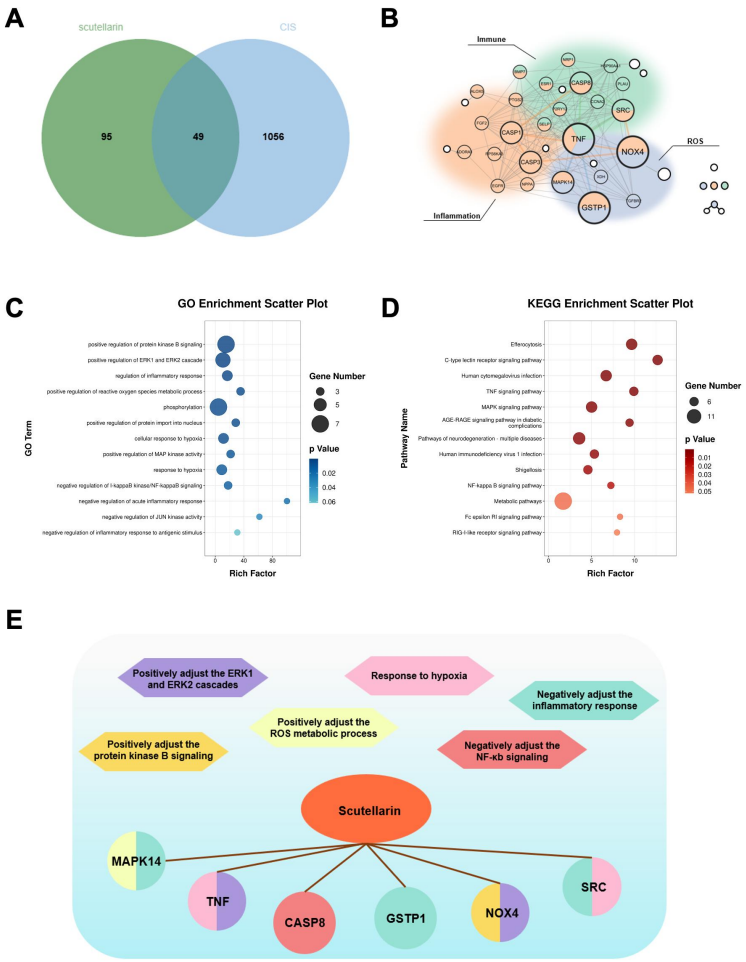

Figure 1 Network pharmacology analysis results. (A) The Venn diagram depicts the intersection of scutellarin target points and ischemic stroke target points. (B) The PPI network diagram of potential targets of scutellarin in the treatment of ischemic stroke. (C) GO analysis. (D) KEGG pathway enrichment analysis. (E) Scutellarin biological functions and biomolecular networks, describing the underlying biological mechanisms of scutellarin. ROS, reactive oxygen species; TNF, tumor necrosis factor; NOX4, NADP(H) oxidase 4; GSTP1, glutathione S-transferase pi 1; SRC, proto-oncogene tyrosine-protein kinase src; MAPK14, mitogen-activated protein kinase 14; CASP8, caspase-8.

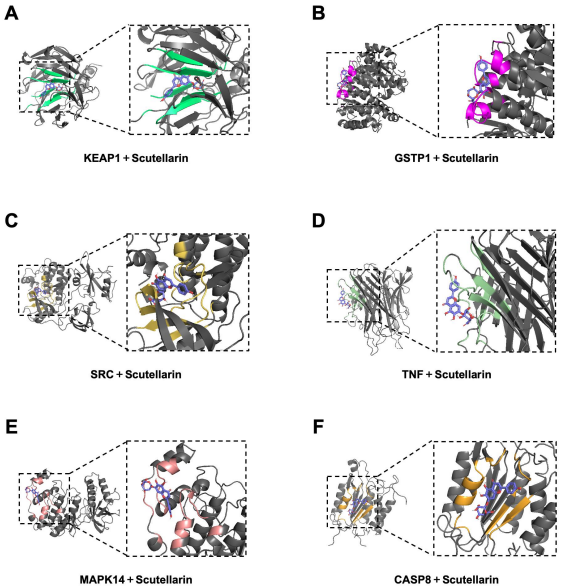

Figure 2 Molecular docking results of scutellarin and six main proteins. (A) Molecular docking results of scutellarin and KEAP1. (B) Molecular docking results of scutellarin and GSTP1. (C) Molecular docking results of scutellarin and SRC. (D) Molecular docking results of scutellarin and TNF. (E) Molecular docking results of scutellarin and MAPK14. (F) Molecular docking results of scutellarin and CASP8. KEAP1, Kelch-like ECH-associated protein 1; GSTP1, glutathione S-transferase pi 1; SRC, proto-oncogene tyrosine-protein kinase src; TNF, tumor necrosis factor; MAPK14, mitogen-activated protein kinase 14; CASP8, caspase-8.

Traditional Medicine Research 2025;10(4):20. https://doi.org/10.53388/TMR20240925001

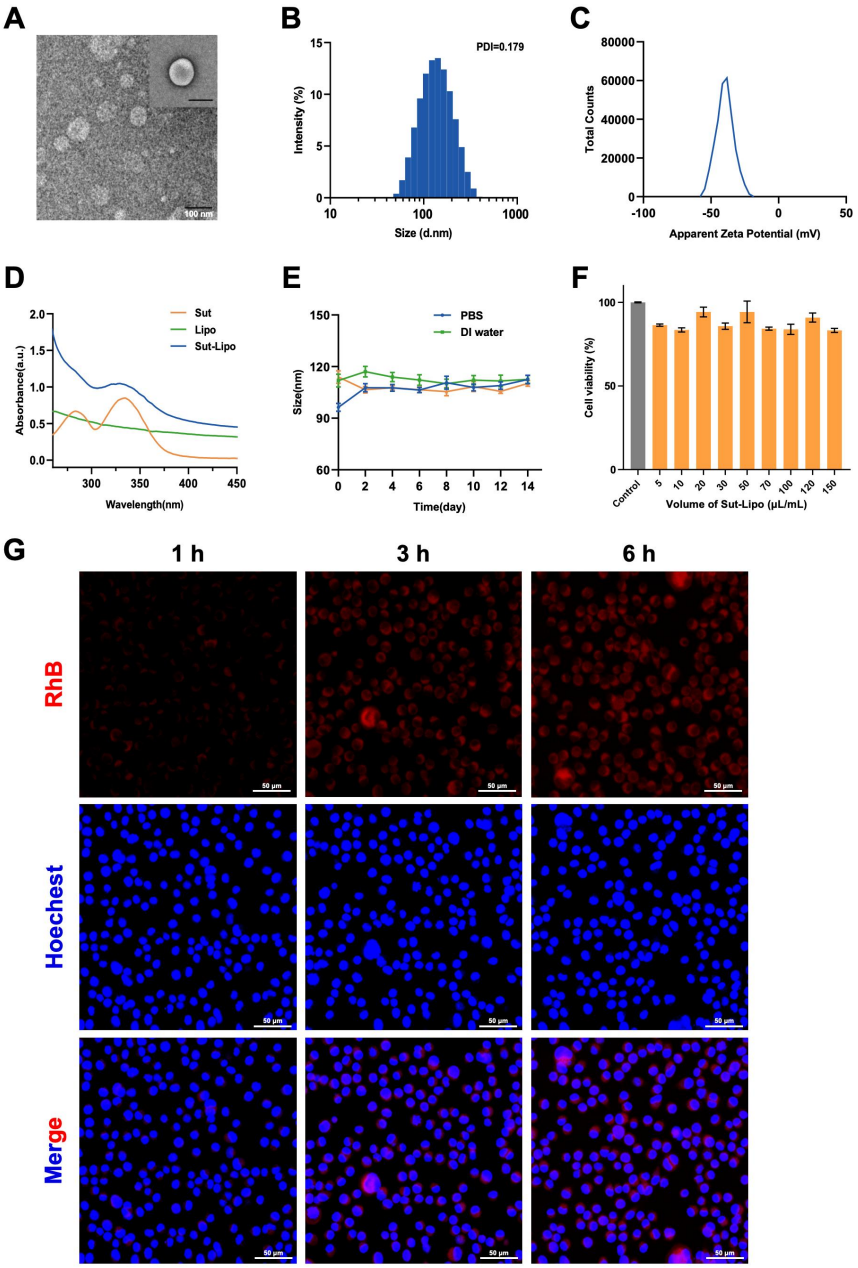

Figure 3 Preparation and characterization of scutellarin liposomes. (A) The TEM images of scutellarin-loaded liposomes. Scale bar = 100 nm (B) Hydrated particle size analysis of scutellarin liposomes. (C) The Zeta potential distribution of scutellarin liposomes. (D) The ultraviolet absorption image of scutellarin with liposomes. (E) The hydration particle size detection of scutellarin liposomes was placed in different solvents over 14 d. (F) The cell viability of HT22 cells treated with scutellarin liposomes of different concentrations. (G) The confocal fluorescence images of HT22 cells effectively take up scutellarin liposomes. Scale bar = 50 μm. PDI, polymer dispersity index; RhB, Rhodamine B.

Scutellarin liposomes-mediated antioxidant cellular assay and assessment of mRNA and protein expression levels

The ability of scutellarin liposomes to reduce intracellular ROS was assessed using the DCFH-DA probe. In the control group, minimal green fluorescence was observed, indicating low basal ROS levels. In contrast, the model group treated with tertiary butyl hydroperoxide showed a significant increase in green fluorescence, reflecting elevated ROS levels and successful induction of oxidative stress (Figure 4A). Treatment with scutellarin liposomes resulted in a marked reduction in green fluorescence, bringing ROS levels close to those of the control group (Figure 4B). These results suggested that scutellarin liposomes effectively alleviate oxidative stress by reducing intracellular ROS levels. In addition, we detected the efficacy of scutellarin liposomes in the oxygen-glucose deprivation/reperfusion model of HT22 cells. The results showed that after treatment, the viability of HT22 cells could be restored to about 89% of the control group at most (Figure 4C).

To explore the mechanism through which scutellarin liposomes reduce intracellular ROS, the expression of antioxidant response element (ARE)-related genes and proteins was examined. Quantitative PCR analysis revealed a significant upregulation of *Hmox1* (2.7-fold) (Figure 4D) and *Nqo1* (2.3-fold) (Figure 4E) gene expression following treatment with scutellarin liposomes. Western blot analysis further demonstrated that there was a substantial increase in the expression of NRF2, HO-1, and NQO1 proteins. Compared to the model group, NRF2 levels increased by 1.6-fold (Figure 4F), HO-1 by 1.5-fold (Figure 4G), and NQO1 by 1.3-fold (Figure 4H). This indicates that scutellarin liposomes activate the KEAP1-NRF2-ARE signaling pathway by inhibiting NRF2 degradation and enhancing the expression of downstream antioxidant proteins.

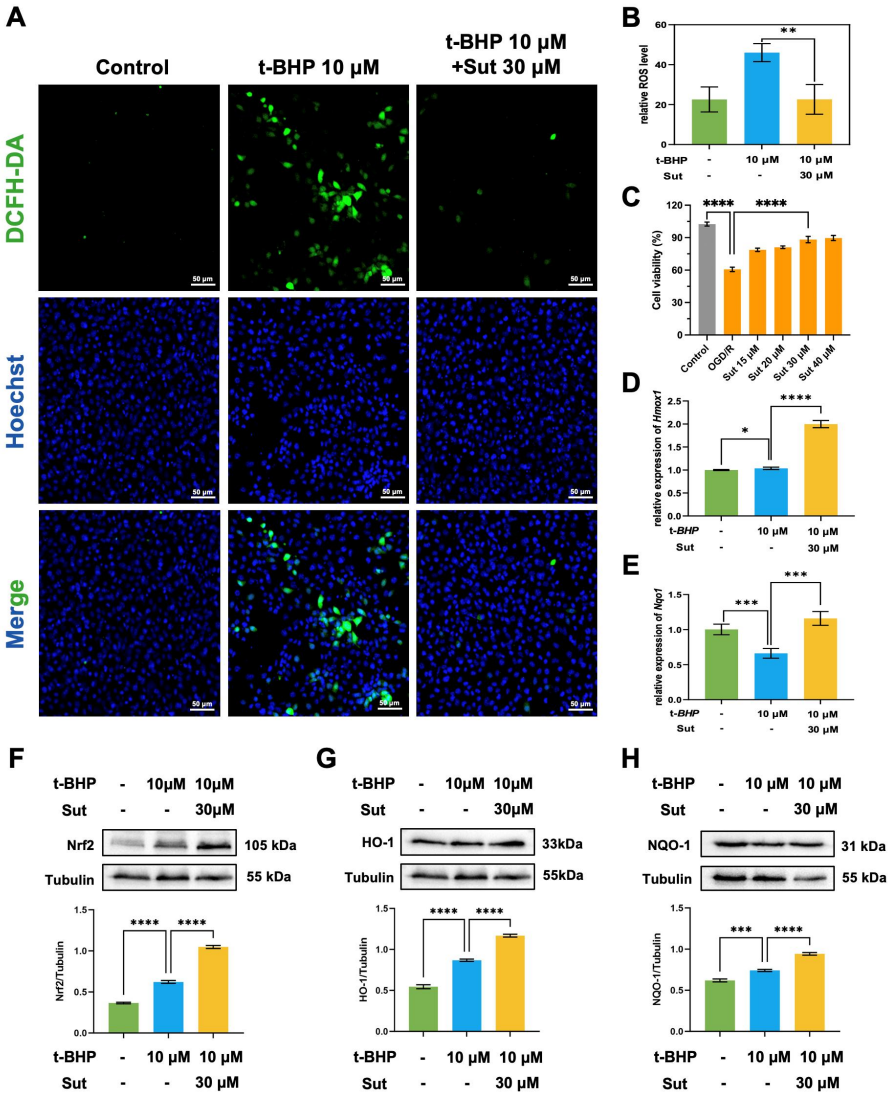

Figure 4 Scutellarin liposomes-mediated antioxidant cellular assay and assessment of mRNA and protein expression levels. (A) The confocal fluorescence images of intracellular ROS in HT22 cells stained with the DCFH-DA probe. Scale bar = 50 μm. (B) Corresponding quantitative analysis of relative ROS level (n = 3). (C) The cell viability of OGD/R HT22 cells treated with scutellarin liposomes of different concentrations. (D) Quantitative analysis of *Hmox1* gene mRNA levels (n = 3). (E) Quantitative analysis of *Nqo1* gene mRNA levels (n = 3). (F) Immunoblotting and quantitative analysis of NRF2 protein (n = 3). (G) Immunoblotting and quantitative analysis of HO-1 protein (n = 3). (H) Immunoblotting and quantitative analysis of NQO1 protein (n = 3). $^{*}P < 0.05$; $^{**}P < 0.01$; $^{***}P < 0.001$; $^{****}P < 0.0001$. ROS, reactive oxygen species; DCFH-DA, 2',7'-Dichlorodihydrofluorescein diacetate; NRF2, nuclear factor E2-related factor 2; NQO1, NAD(P)H quinone dehydrogenase 1; HO-1, heme oxygenase 1; t-BHP, tert-butyl hydroperoxide; Sut, scutellarin.

Experimental validation that scutellarin is a non-covalent inhibitor of the KEAP1-NRF2 interaction

A ligand fishing experiment was conducted to identify intracellular proteins interacting with scutellarin. Scutellarin was immobilized on epoxy-functionalized microspheres, followed by incubation with lysed cell extracts (Figure 5A). Unbound proteins were washed away, and the bound proteins were analyzed using SDS-PAGE and silver staining (Figure 5B). Mass spectrometry of the enriched proteins identified KEAP1 as a significantly enriched target, suggesting a direct interaction between scutellarin and KEAP1.

We purified both the wild-type Kelch domain and a mutant variant of the protein. The mutant Kelch domain included substitutions at key residues (Y334A, R380A, N382A, N414A, R415A, Y572A, and S602A), which are known to be critical for binding with NRF2 and conventional KEAP1 inhibitors. To assess the binding affinity of scutellarin with these Kelch domains, we utilized Bio-Layer Interferometry. The results revealed that Scutellarin binds to the wild-type Kelch domain with an affinity of 26.10 μM (R^2 = 0.99). However, the binding affinity to the mutant Kelch domain was significantly reduced (Figure 5C).

The interaction between KEAP1 and NRF2 was further confirmed using co-immunoprecipitation assays. Cells transfected with KEAP1-Flag were incubated with scutellarin, and the resulting complexes were immunoprecipitated using anti-Flag magnetic beads. In the absence of scutellarin, NRF2 was readily co-precipitated with KEAP1. However, upon scutellarin treatment, the amount of NRF2 associated with KEAP1 decreased by over 50%, indicating that scutellarin effectively disrupts the KEAP1-NRF2 interaction (Figure 5D).

Hydrogen-deuterium exchange mass spectrometry was performed to investigate the structural changes in the Kelch domain of KEAP1 upon scutellarin binding. Significant increases in deuterium exchange were observed in the peptide segments L342-L355, S555-I566, and D394-G423, indicating that scutellarin binding induces conformational changes that expose these regions on the protein surface (Figure 5E).

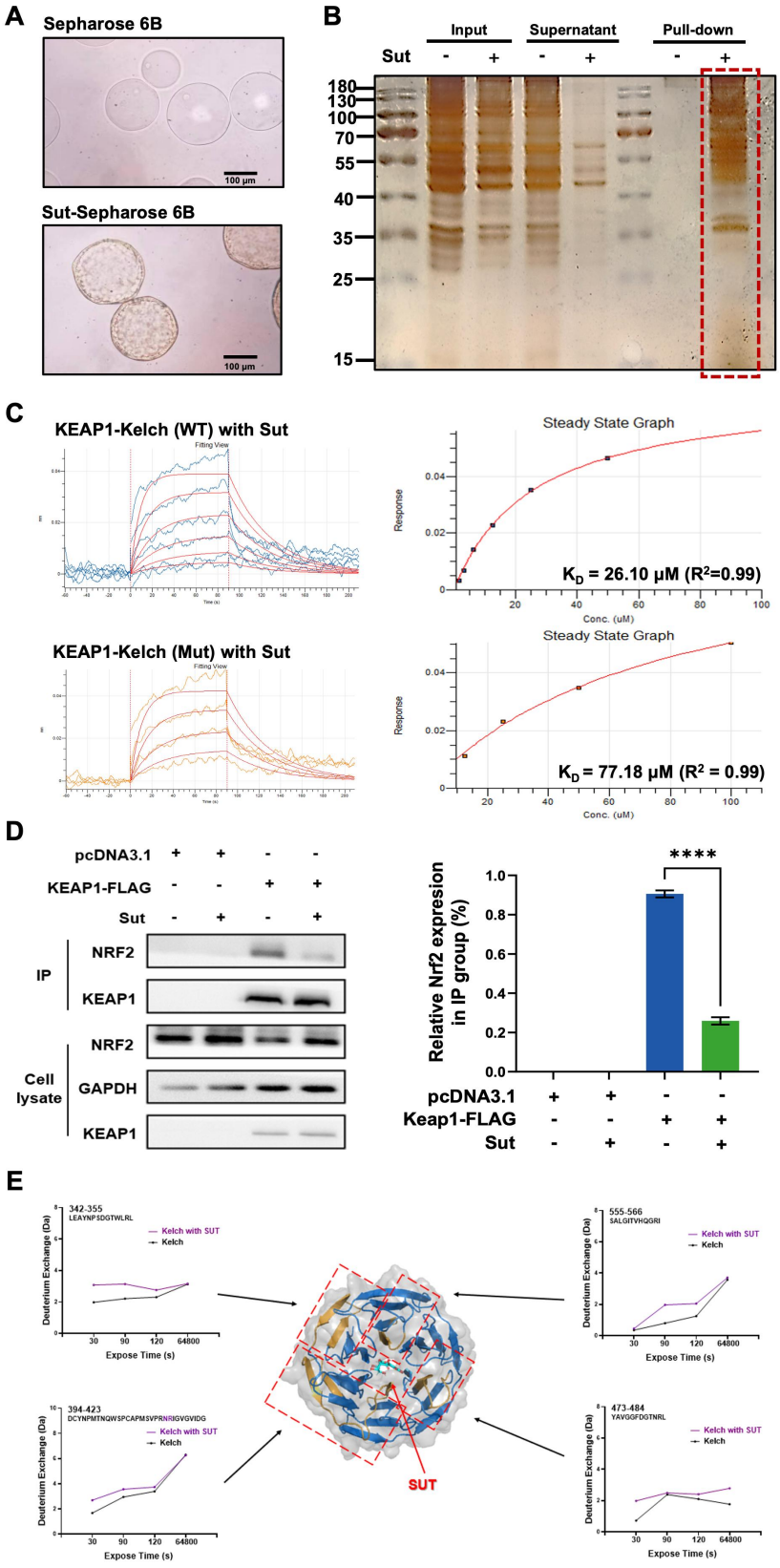

Figure 5 Experimental validation that scutellarin is a non-covalent inhibitor of the KEAP1-NRF2 interaction. (A) Microspheres before and after binding with scutellarin. Scale bar = 100 μm. (B) SDS-PAGE Silver staining image. (C) In vitro detection of KEAP1-Kelch domain with scutellarin using BLI. (D) In HEK 293T cells, the effect of scutellarin on the KEAP1-NRF2 interaction was assessed: Left: Co-IP results diagram; Right: Quantitative analysis of NRF2 content variation. (E) The hydrogen-deuterium exchange mass spectrometry results and binding schematic diagram of scutellarin with the Kelch domain of KEAP1. $^{****}P < 0.0001$. KEAP1, Kelch-like ECH-associated protein 1; NRF2, nuclear factor E2-related factor 2; Sut, scutellarin; Mut, mutant variant; GAPDH, glyceraldehyde-3-phosphate dehydrogenase; WT, wild-type.

Discussion

Scutellarin, a flavonoid compound, is a bioactive component found in traditional Chinese medicines such as *Scutellaria baicalensis* and *Lamprocapnos spectabilis*. Scutellarin is a potential drug for combating oxidative stress damage in various diseases; however, its direct target protein has not yet been identified. The core finding of this study is the development of scutellarin-based liposomes as an antioxidant switch to mitigate neuronal damage caused by ischemic stroke. Moreover, its direct target protein and mechanism of action have been demonstrated. The research shows that these scutellarin liposomes can significantly reduce intracellular ROS levels, alleviate oxidative stress, and activate downstream antioxidant factors such as HO-1 and NQO1 by upregulating NRF2 protein, thereby providing neuroprotective effects and resisting OGD/R injury. Furthermore, experimental results confirmed the direct binding of scutellarin to the KEAP1 protein through co-immunoprecipitation and HDX-MS, revealing that it allosterically regulates KEAP1 and influences its interaction with NRF2.

The novelty of this study lies in the combination of the traditional Chinese medicine component scutellarin with modern nanomedicine delivery systems (liposomes), which not only improves the bioavailability and compatibility of scutellarin but also overcomes its limitations of poor water solubility and short half-life. Additionally, the study delves into the role of scutellarin in the antioxidant mechanisms, particularly in the KEAP1-NRF2 signaling pathway, providing new insights and methods for treating neurodegenerative diseases such as stroke.

Scutellarin has limitations in clinical application due to its poor water solubility, low bioavailability, and short half-life. To overcome these drawbacks, we developed scutellarin-loaded liposomes to improve the drug's stability and biocompatibility. Our experimental results show that these liposomes have a uniform particle size distribution, good stability, and high encapsulation efficiency. Toxicity assays and endocytosis studies in HT22 cells indicate that these liposomes are effectively internalized and exhibit low toxicity within the tested concentration range, providing a solid foundation for further research. Ischemic stroke injury is mainly caused by excessive intracellular accumulation of ROS, which leads to significant damage to cellular structures and DNA. To evaluate scutellarin's therapeutic potential in ischemic stroke, we assessed its antioxidant efficacy at the cellular level. Our findings demonstrated that scutellarin liposomes significantly reduced ROS levels in induced cells, confirming their antioxidant capacity.

The KEAP1-NRF2-ARE signaling pathway is a crucial defense mechanism against oxidants and xenobiotics. In normal conditions, KEAP1 homodimers bind to NRF2, leading to its ubiquitination and subsequent proteasomal degradation, thus preventing NRF2 from translocating to the nucleus. However, during oxidative stress, this interaction is disrupted, enabling NRF2 to escape degradation, move to the nucleus, and bind to the ARE element, which in turn promotes the expression of antioxidant genes like *Hmox1* and *Nqo1*. We hypothesize that scutellarin directly interacts with the Kelch domain of KEAP1, allosterically modulating its interaction with NRF2. This is likely to enhance the expression of downstream antioxidant elements such as HO-1 and NQO1, reducing intracellular ROS levels and alleviating cellular oxidative stress. Co-immunoprecipitation, ligand fishing experiments, and Bio-layer interferometry assays confirmed that scutellarin disrupts the KEAP1-NRF2 interaction by binding to the KEAP1 Kelch domain. These findings were supported by HDX-MS experiments. We validated the molecular mechanism of scutellarin through multiple analyses. At the mRNA and protein levels, studies showed that scutellarin liposomes significantly upregulated the expression of *Hmox1* and *Nqo1* genes. Additionally, NRF2, HO-1, and NQO1 proteins were also significantly increased, while KEAP1 expression remained relatively unchanged.

Despite the achievements of this study, several limitations exist. The research scope is limited, mainly concentrating on cell experiments and lacking comprehensiveness for the whole animal model and in vivo environment. Although scutellarin based liposomes show potential in cell experiments, there is insufficient exploration of potential treatment method limitations such as long-term safety and drug interactions in clinical applications. For future directions, an in-depth study of the mechanism is required. This includes understanding its role in ischemic stroke treatment through details with KEAP1-NRF2-ARE and other relevant pathways. The drug delivery system should be optimized considering scutellarin's properties. This can be achieved by improving liposomes or exploring other methods to enhance solubility, bioavailability, and stability. In vivo experiments need to be conducted to study pharmacokinetics, pharmacodynamics, treatment effects, and safety, providing a basis for clinical applications.

References

1. Tsao CW, Aday AW, Almarzooq ZI, et al. Heart Disease and Stroke Statistics-2023 Update: A Report From the American Heart Association. *Circulation.* 2023;147(8):e93–e621. Available at: http://doi.org/10.1161/CIR.0000000000001123
2. Feigin VL, Brainin M, Norrving B, et al. World Stroke Organization (WSO): Global Stroke Fact Sheet 2022. *Int J Stroke.* 2022;17(1):18–29. Available at: http://doi.org/10.1177/17474930211065917
3. Tu WJ, Wang LD. Special Writing Group of China Stroke Surveillance Report. China stroke surveillance report 2021. *Mil Med Res.* 2023;10(1):33. Available at: http://doi.org/10.1186/s40779-023-00463-x
4. Alsbrook DL, Di Napoli M, Bhatia K, et al. Neuroinflammation in Acute Ischemic and Hemorrhagic Stroke. *Curr Neurol Neurosci Rep.* 2023;23(8):407–431. Available at: http://doi.org/10.1007/s11910-023-01282-2
5. Candelario-Jalil E, Dijkhuizen RM, Magnus T. Neuroinflammation, Stroke, Blood-Brain Barrier Dysfunction, and Imaging Modalities. *Stroke.* 2022;53(5):1473–1486. Available at: http://doi.org/10.1161/STROKEAHA.122.036946
6. Qin C, Yang S, Chu YH, et al. Signaling pathways involved in ischemic stroke: molecular mechanisms and therapeutic interventions. *Signal Transduct Target Ther.* 2022;7(1):215. Available at: http://doi.org/10.1038/s41392-022-01064-1
7. Gallego I, Villate-Beitia I, Saenz-del-Burgo L, Puras G, Pedraz JL. Therapeutic Opportunities and Delivery Strategies for Brain Revascularization in Stroke, Neurodegeneration, and Aging. *Pharmacol Rev.* 2022;74(2):439–461. Available at: http://doi.org/10.1124/pharmrev.121.000418
8. Korczowska-Łącka I, Hurła M, Banaszek N, et al. Selected Biomarkers of Oxidative Stress and Energy Metabolism Disorders in Neurological Diseases. *Mol Neurobiol.* 2023;60(7):4132–4149. Available at: http://doi.org/10.1007/s12035-023-03329-4
9. Mead GE, Sposato LA, Sampaio Silva G, et al. A systematic review and synthesis of global stroke guidelines on behalf of the World Stroke Organization. *Int J Stroke.* 2023;18(5):499–531. Available at: http://doi.org/10.1177/17474930231156753
10. Zhao Y, Zhang X, Chen X, Wei Y. Neuronal injuries in cerebral infarction and ischemic stroke: From mechanisms to treatment (Review). *Int J Mol Med.* 2021;49(2):15. Available at: http://doi.org/10.3892/ijmm.2021.5070
11. Du Y, Huo Y, Yang Q, et al. Ultrasmall iron-gallic acid coordination polymer nanodots with antioxidative neuroprotection for PET/MR imaging-guided ischemia stroke therapy. *Exploration (Beijing).* 2023;3(1):20220041. Available at: http://doi.org/10.1002/EXP.20220041

12. Tsivgoulis G, Katsanos AH, Sandset EC, et al. Thrombolysis for acute ischaemic stroke: current status and future perspectives. *Lancet Neurol.* 2023;22(5):418–429. Available at: http://doi.org/10.1016/S1474-4422(22)00519-1
13. Tan YQ, Lin F, Ding YK, et al. Pharmacological properties of total flavonoids in Scutellaria baicalensis for the treatment of cardiovascular diseases. *Phytomedicine.* 2022;107:154458. Available at: http://doi.org/10.1016/j.phymed.2022.154458
14. Guo C, Huang Q, Wang Y, et al. Therapeutic application of natural products: NAD^+ metabolism as potential target. *Phytomedicine.* 2023;114:154768. Available at: http://doi.org/10.1016/j.phymed.2023.154768
15. Yang H, Wang Z, Wang L, et al. Scutellarin ameliorates osteoarthritis by protecting chondrocytes and subchondral bone microstructure by inactivating NF-κB/MAPK signal transduction. *Biomed Pharmacother.* 2022;155:113781. Available at: http://doi.org/10.1016/j.biopha.2022.113781
16. Zhang X, Dong Z, Fan H, et al. Scutellarin prevents acute alcohol-induced liver injury via inhibiting oxidative stress by regulating the Nrf2/HO-1 pathway and inhibiting inflammation by regulating the AKT, p38 MAPK/NF-κB pathways. *J Zhejiang Univ Sci B.* 2023;24(7):617–631. Available at: http://doi.org/10.1631/jzus.B2200612
17. Mei XY, Zhang JN, Jia WY, et al. Scutellarin suppresses triple-negative breast cancer metastasis by inhibiting TNFα-induced vascular endothelial barrier breakdown. *Acta Pharmacol Sin.* 2022;43(10):2666–2677. Available at: http://doi.org/10.1038/s41401-022-00873-y
18. Zhou L, Han Y, Yang Q, et al. Scutellarin attenuates doxorubicin-induced oxidative stress, DNA damage, mitochondrial dysfunction, apoptosis and autophagy in H9c2 cells, cardiac fibroblasts and HUVECs. *Toxicol In Vitro.* 2022;82:105366. Available at: http://doi.org/10.1016/j.tiv.2022.105366
19. Su YM, Fan XM, Li SM, Li ZG, Tian M, Li SD. Scutellarin Improves Type 2 Diabetic Cardiomyopathy by Regulating Cardiomyocyte Autophagy and Apoptosis. *Dis Markers.* 2022;2022:3058354. Available at: http://doi.org/10.1155/2022/3058354
20. Sun XP, Zhou L, Han YL, et al. Scutellarin Attenuates Doxorubicin-Induced Cardiotoxicity by Inhibiting Myocardial Fibrosis, Apoptosis and Autophagy in Rats. *Chem Biodivers.* 2022;20(1):e202200450. Available at: http://doi.org/10.1002/cbdv.202200450
21. Yu P, Li J, Luo Y, et al. Mechanistic Role ofScutellaria baicalensisGeorgi in Breast Cancer Therapy. *Am J Chin Med.* 2023;51(2):279–308. Available at: http://doi.org/10.1142/S0192415X23500155
22. Fang HY, Zhao XN, Zhang M, Ma YY, Huang JL, Zhou P. Beneficial effects of flavonoids on cardiovascular diseases by influencing NLRP3 inflammasome. *Inflammopharmacology.* 2023;31(4):1715–1729. Available at: http://doi.org/10.1007/s10787-023-01249-2
23. Tuli HS, Bhushan S, Kumar A, et al. Autophagy Induction by Scutellaria Flavones in Cancer: Recent Advances. *Pharmaceuticals (Basel).* 2023;16(2):302. Available at: http://doi.org/10.3390/ph16020302
24. Vesaghhamedani S, Mazloumi Kiapey SS, Gowhari Shabgah A, et al. From traditional medicine to modern oncology: Scutellarin, a promising natural compound in cancer treatment. *Prog Biophys Mol Biol.* 2023;180–181:19–27. Available at: http://doi.org/10.1016/j.pbiomolbio.2023.04.006
25. Nsairat H, Khater D, Sayed U, Odeh F, Al Bawab A, Alshaer W. Liposomes: structure, composition, types, and clinical applications. *Heliyon.* 2022;8(5):e09394. Available at: http://doi.org/10.1016/j.heliyon.2022.e09394
26. Lombardo D, Kiselev MA. Methods of Liposomes Preparation: Formation and Control Factors of Versatile Nanocarriers for Biomedical and Nanomedicine Application. *Pharmaceutics.* 2022;14(3):543. Available at: http://doi.org/10.3390/pharmaceutics14030543
27. Dilliard SA, Siegwart DJ. Passive, active and endogenous organ-targeted lipid and polymer nanoparticles for delivery of genetic drugs. *Nat Rev Mater.* 2023;8(4):282–300. Available at: http://doi.org/10.1038/s41578-022-00529-7
28. Bai X, Kang J, Wei SL, et al. A pH responsive nanocomposite for combination sonodynamic-immunotherapy with ferroptosis and calcium ion overload via SLC7A11/ACSL4/LPCAT3 pathway. *Exploration.* 2024;20240002. Available at: http://doi.org/10.1002/EXP.20240002
29. Hersh AM, Alomari S, Tyler BM. Crossing the Blood-Brain Barrier: Advances in Nanoparticle Technology for Drug Delivery in Neuro-Oncology. *Int J Mol Sci.* 2022;23(8):4153. Available at: http://doi.org/10.3390/ijms23084153
30. Gao Q, Feng J, Liu W, et al. Opportunities and challenges for co-delivery nanomedicines based on combination of phytochemicals with chemotherapeutic drugs in cancer treatment. *Adv Drug Deliv Rev.* 2022;188:114445. Available at: http://doi.org/10.1016/j.addr.2022.114445
31. Dymek M, Sikora E. Liposomes as biocompatible and smart delivery systems – the current state. *Adv Colloid Interface Sci.* 2022;309:102757. Available at: http://doi.org/10.1016/j.cis.2022.102757
32. Nakamura T, Sato Y, Yamada Y, et al. Extrahepatic targeting of lipid nanoparticles in vivo with intracellular targeting for future nanomedicines. *Adv Drug Deliv Rev.* 2022;188:114417. Available at: http://doi.org/10.1016/j.addr.2022.114417